Front. Optoelectron. 2021, 14(2): 221–228
https://doi.org/10.1007/s12200-019-0921-6

RESEARCH ARTICLE

Polarization-sensitive and active controllable electromagnetically induced transparency in U-shaped terahertz metamaterials

Kun REN (✉)[1], Ying ZHANG[1], Xiaobin REN[2], Yumeng HE[1], Qun HAN[1]

1 College of Precision Instrument and Opto-electronics Engineering, Tianjin University; Key Laboratory of Opto-electronics Information Technology, Ministry of Education, Tianjin 300072, China
2 School of Science, Tianjin University of Science and Technology, Tianjin 300222, China

Abstract Electromagnetically induced transparency (EIT) phenomenon is observed in simple metamaterial which consists of concentric double U-shaped resonators (USRs). The numerical and theoretical analysis reveals that EIT arises from the bright-bright mode coupling. The transmission spectra at different polarization angle of incident light shows that EIT transparency window is polarization sensitive. More interestingly, Fano resonance appears in the transmission spectrum at certain polarization angles. The sharp and asymmetric Fano lineshape is high valuable for sensing. The performance of sensor is investigated and the sensitivity is high up to 327 GHz/RIU. Furthermore, active control of EIT window is realized by incorporating photosensitive silicon. The proposed USR structure is simple and compact, which may find significant applications in tunable integrated devices such as biosensor, filters, and THz modulators.

Keywords electromagnetically induced transparency (EIT), metamaterial, polarization-sensitive, active optical devices, sensor

1 Introduction

Electromagnetically induced transparency (EIT) was initially found in atomic system. EIT originates from quantum interference, which causes the decrease of absorption and produces transparent peak at the absorption frequency [1–3]. EIT has interesting applications in slow light technology [4], optical communication [5], optical switch [6,7], and signal transmission [8]. However, the strictly experimental conditions, such as ultra-low temperature, strong magnetic field and high-power laser, have greatly limited the applications of EIT.

Metamaterials are artificially electromagnetic materials which have unique properties, such as negative permeability [9], small antenna [10,11], perfect lens [12], invisibility cloak [13,14], and metamaterial absorber [15–17]. Those properties are impossible to acquire by use of naturally materials. Plasmonic analog of EIT phenomenon achieved in metamaterials is usually called plasmon-induced transparency (PIT) [18,19]. The bright-bright and bright-dark mode couplings are generally studied in metamaterials [20–22]. The bright mode with low quality factor can be directly coupled by the external field. On the contrary, the dark mode with high quality factor cannot be excited except through the coupling of bright mode [23,24]. The bright and dark modes resonate at the same frequency. The necessary condition to achieve PIT is their contrasting linewidths. For example, EIT-like effect was obtained by a cut wire and two oppositely oriented split ring resonators though bright-dark mode coupling [25]. PIT has been demonstrated by graphene ring and strip resonators though bright-bright mode coupling [26]. The frequency detuning is needed for PIT effect based on bright-bright coupling. Very recently, EIT-like effect based on a bright-dark-bright coupling was reported [27]. It is demonstrated that transparency window of EIT-like effect can be tuned by changing the structural parameters of metamaterials [28]. However, the reconstruction of structure is complicated. It is necessary to dynamically modulate EIT-like effect. Active control of the transparency window by applied voltage or by thermal actuation are proposed [29–31].

In this paper, the number of EIT peaks can be controlled by changing the polarization of incident light. The proposed planar metamaterial is composed of concentric

Received April 4, 2019; accepted June 18, 2019

E-mail: renkun@tju.edu.cn

double U-shaped resonators (USRs). Moreover, when silicon bar is added to the USR, the amplitude of EIT peaks can be modulated by changing optical power. The designed structure suggests applications in tunable THz modulator, biosensor.

2 Structure design and theoretical model

Figure 1 shows one period unit of the proposed metamaterial, which consists of concentric double USRs. The lengths of outer and inner USRs are a = 140 μm, b = 105 μm, respectively. The widths of outer and inner USRs are $w_1 = w_2$ = 10 μm. The distance between the two USRs is s = 7.5 μm. The periods along x- and y-axis are $P_x = P_y$ = 160 μm. The yellow part stands for copper, whose thickness is 3 μm. The relative permittivity of copper is given by $\varepsilon_m(\omega) = \varepsilon_\infty - \omega_p^2/(\omega^2 + i\omega\gamma_p)$, where $\varepsilon_\infty = 1$ and ε_∞ is the dielectric constant. The angle frequency of the incident light is ω and plasma frequency is $\omega_p = 6.03 \times 10^{15}$ rad/s. The damping rate $\gamma_p = 5.56 \times 10^{13}$ rad/s. The relative permittivity of the substrate is 1.98 and the thickness of the substrate is h_1 = 50 μm. In this paper, the EIT-like effect of metamaterial is numerically studied by COMSOL Multiphysics software. Periodical boundary conditions in xOz and yOz planes are adopted. The extremely fine mesh is used to discretize the space and ensure the convergence of the calculated results. Floquet ports are added on the top and bottom faces of the simulation space.

Theoretical analyzation is done based on coupled Lorentz oscillator (CLO) model [32,33]. The displacements vectors for particles 1 and 2 are $x_1 = c_1\exp(i\omega_1 t)$ and $x_2 = c_2\exp(i\omega_2 t)$. We consider two particles interacting with the incident electric field $E = E_0\exp(i\omega t)$, which can be described by the following equations:

$$\ddot{x}_1(t) + \gamma_1\dot{x}_1(t) + \omega_1^2 x_1(t) + \Omega^2 x_2(t) = \frac{Q}{M}E, \quad (1)$$

$$\ddot{x}_2(t) + \gamma_2\dot{x}_2(t) + \omega_2^2 x_2(t) + \Omega^2 x_1(t) = \frac{q}{m}E, \quad (2)$$

where (ω_1, ω_2) and (γ_1, γ_2) are resonance angular frequencies and loss factors of the bright and the quasi-dark modes, respectively. Ω stands for the coupling strength between the bright and quasi-dark particles. (Q, q) and (M,m) are effective charge and effective mass, respectively. External forces are denoted by $f_1 = Q/M$ and $f_2 = q/m$, which means free space coupling strengths of bright and quasi-dark modes with the incoming light. Dimensionless constants A and B are defined to describe the relative coupling of incident light with bright and quasi-dark modes $A = Q/q$ and $B = M/m$.

Solving the above coupled equations, we obtain

$$x_1 = \frac{\frac{B}{A}\Omega^2 + (\omega^2 - \omega_2^2 + i\omega\gamma_2)}{\Omega^4 - (\omega^2 - \omega_1^2 + i\omega\gamma_1)(\omega^2 - \omega_2^2 + i\omega\gamma_2)}\frac{Q}{M}E_0, \quad (3)$$

$$x_2 = \frac{\Omega^2 + \frac{B}{A}(\omega^2 - \omega_1^2 + i\omega\gamma_1)}{\Omega^4 - (\omega^2 - \omega_1^2 + i\omega\gamma_1)(\omega^2 - \omega_2^2 + i\omega\gamma_2)}\frac{Q}{M}E_0. \quad (4)$$

The linear susceptibility (χ) is then written as

$$\chi = \frac{k}{A^2 B}\left(\frac{A(B+1)\Omega^2 + A^2\left((\omega^2 - \omega_2^2) + B(\omega^2 - \omega_1^2)\right)}{\Omega^4 - (\omega^2 - \omega_1^2 + i\omega\gamma_1)(\omega^2 - \omega_2^2 + i\omega\gamma_2)}\right.$$

$$\left. + i\omega\frac{A^2\gamma_2 + B\gamma_1}{\Omega^4 - (\omega^2 - \omega_1^2 + i\omega\gamma_1)(\omega^2 - \omega_2^2 + i\omega\gamma_2)}\right). \quad (5)$$

The transmission coefficient (T) is obtained from $T = 1 - \mathrm{Im}(\chi)$.

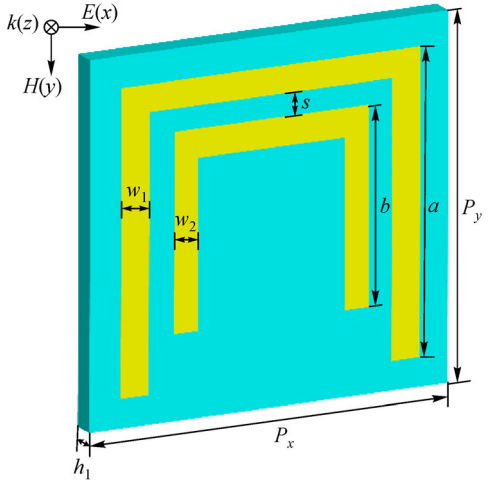

Fig. 1 Schematic diagram of a unit cell consisting of concentric double USRs. $P_x = P_y$ = 160 μm, a = 140 μm, b = 105 μm, $w_1 = w_2$ = 10 μm, s = 7.5 μm, h_1 = 50 μm

3 Results and discussion

The incident light propagates along z direction and enters the metal plane at normal incidence. The electric field E is oriented along x-axis. The simulated results are plotted in Fig. 2. When a unit cell consists of only one USR, there is a dip in the transmission spectrum, as shown in Figs. 2(a) and 2(b). The corresponding resonant frequency is 0.32 THz for outer USR and 0.45 THz for inner USR. Both modes can be excited directly by the incident light. Considering their small difference in linewidth, we regard them as bright modes. The resonance frequency has a blue shift with the decrease of USR dimension. This can be explained by resonance function. It is given by the

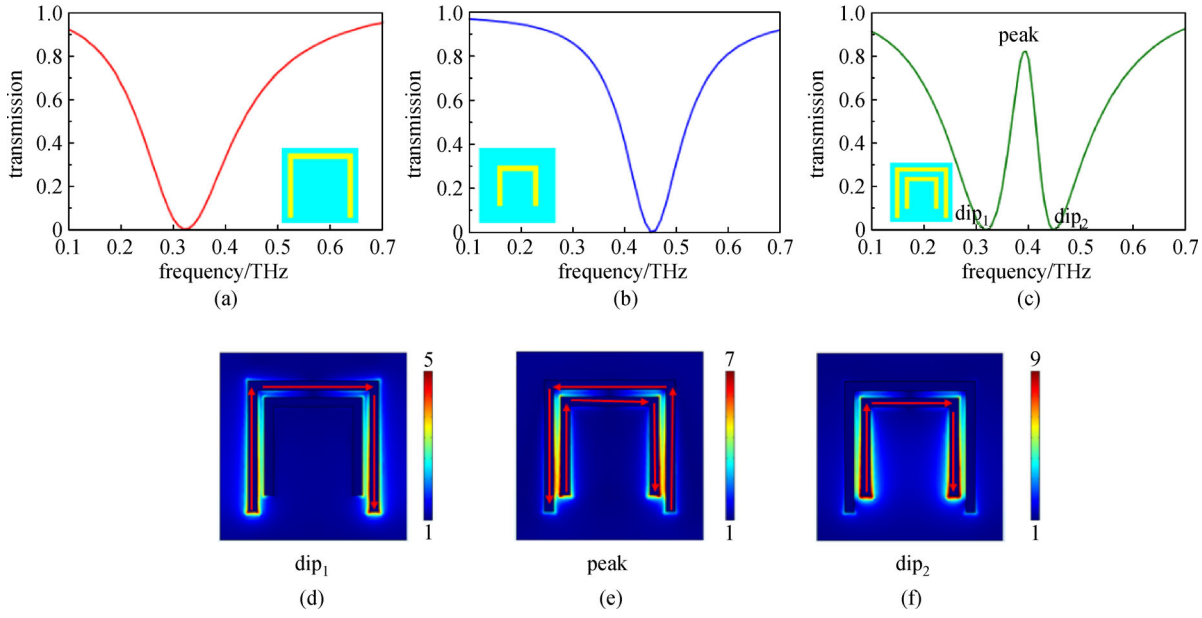

Fig. 2 Transmission spectra for (a) only the outer USR, (b) only the inner USR, and (c) concentric double USRs. The electric field distribution of concentric double USR for (d) dip_1 at 0.32 THz, (e) peak at 0.395 THz and (f) dip_2 at 0.45 THz

following simple relation:

$$\omega_0 \mathrm{Re}(n_{\mathrm{eff}}) L_{\mathrm{eff}}/c + \varphi_r = 2m\pi, \tag{6}$$

where ω_0 is the resonant frequency of the cavity. $\mathrm{Re}(n_{\mathrm{eff}})$ is the real part of effective index for surface plasmon polaritons in USR. L_{eff} denotes the effective cavity length for one trip in USR. φ_r means the phase shift caused by the reflection on the USR facets during one trip. Positive integer m stands for the order of resonant mode. Equation (6) shows that the resonance frequency becomes bigger with the decrease of USR length. This analysis agrees with the above simulation.

Figure 2(c) shows the transmission spectrum of concentric double USRs. It is observed that a transparency window appears among two dips. EIT-like phenomenon is observed. Two dips are denoted by dip_1 and dip_2 whose frequencies are 0.32 and 0.45 THz, respectively. The peak frequency is 0.395 THz. The highest transmittance is up to 0.82. To further understand the intrinsic mechanism of EIT characteristic, the distribution of electric field is displayed in Figs. 2(d) and 2(f), in which red arrows show the direction of the surface current. The electric field distribution at dip_1 shows that strong field energy is located around the outer USR. The current density in outer USR is greater than that in inner USR. At the frequency of dip_2, field energy is mainly confined in the inner USR, and the current density in the inner USR is more intense. The directions of current flow at two dip frequencies are clockwise. At peak frequency, the energy is confined in the area between two USRs. The redistribution of energy implies that the field in the outer USR has an influence on the field in the inner USR by near field coupling. The direction of surface current in inner USR keeps clockwise while the surface current in the outer USR is counter-clockwise. The coupling between the bright and bright resonators leads to the induced transparency window.

The influence of USR dimension on EIT transmission spectrum is investigated. Figure 3 shows the transmission spectrum under different length a and b of USRs. As the length a increases, dip_1 gradually moves to lower frequency and dip_2 remains unchanged. Meanwhile, the amplitude of peak increases. With the increase of b, the position of dip_1 does not change, but dip_2 has a redshift. The transmittance of peak gradually decreases. This phenomenon can be explained based on the energy distribution of field. Figures 2(d) and 2(f) indicate the position of dip_1 is more affected by the outer USR and dip_2 is more affected by the inner USR. Moreover, Eq. (1) shows that the resonance frequency is dependent on the length of cavity.

The CLO model is adopted to analyze tunable transmission property in Fig. 3. Because of the increased length a (or b), the resonance frequency ω_1 (or ω_2) will decrease. We theoretically analyze the evolution of transmission with frequencies ω_1 and ω_2. When resonance frequencies ω_1 and ω_2 vary with USR dimension, the loss factors of resonators used in the fitting change. The fitted transmission spectrums are plotted in Fig. 4. The analytical results are in good agreement with the numerically simulated results. As ω_1 increases, dip_1 gradually moves to high frequency and dip_2 remains unchanged. With the increase of ω_2, the position of dip_1 does not change, but dip_2 moves to high frequency.

The utilization of THz wave in biosensor attracts much

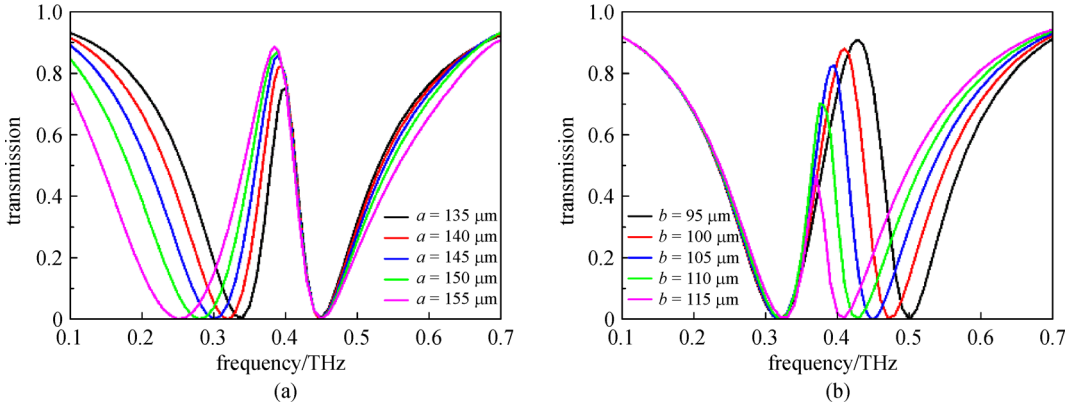

Fig. 3 Simulated transmission spectrum with different lengths of USR. (a) Length a of outer USR; (b) length b of inner USR. The other geometric parameters remain unchanged

attention because of its non-destructive detection of cells. Normally refractive index sensors rely on the change of optical properties caused by the variation in refractive index of detection objects. Narrow EIT-like lineshape in metamaterial has the advantage of improved sensitivity. To study the sensing performance, different analytes are placed on metamaterials. The obtained transmission spectra are presented in Fig. 5(a). The variations in refractive index produce the shift in position of EIT-like peak. The frequencies of dip_1/peak/dip_2 shift from 0.320 to 0.305 THz, 0.395 to 0.380 THz, and 0.450 to 0.435 THz, respectively. They show a trend of redshift when the refractive index increases from 1.00 to 1.06. Figure 5(b) presents the resonance frequency changes of refractive index of the analyte. The frequency shift of the dip_1/peak/dip_2 is approximately linearly related to refractive index. The sensitivity of refractive index sensor is defined by $S = \Delta f / \Delta n$ [34], which denotes the change in frequency of the unit refractive index (RIU). For dip_1/peak/dip_2, the obtained sensitivity S are 250, 250, 250 GHz/RIU, respectively. The sensitivity is comparable to previously reported THz metamaterial sensors [35,36].

Table 1 presents the comparison of our sensor with those previously reported. Considering the working frequencies of sensors are different, we define relative sensitivity to evaluate the sensing performance: $S^* = S/f_0$, where f_0 is the resonance frequency. The working frequency band, refractive index sensitivity S, and relative sensitivity S^* are given. Our proposed sensor has good sensing performance.

Figure 6(a) shows the transmission spectrum at different polarization angle. It is obvious that EIT-like effect is polarization-sensitive. For y-polarized THz field (corresponding to $\theta = 90°$), EIT transparency window can still be observed but it has a blueshift about 0.365 THz compared with that of x-polarization ($\theta = 0°$). At other polarization angles, multiple transparency windows and dips are observed. This provides a simple method to obtain multi-channel filtering since it does not need the reconfiguration of geometry. Furthermore, asymmetric lineshape appears around 0.81 THz as the polarization angle changes from 30° to 75°. This kind of lineshape is the typical characteristic of Fano resonance [39]. We attribute the generation of Fano resonance to the combined effect of x-polarized and y-polarized incident light. Take the example of $\theta = 45°$. In this case, electric field will decompose into

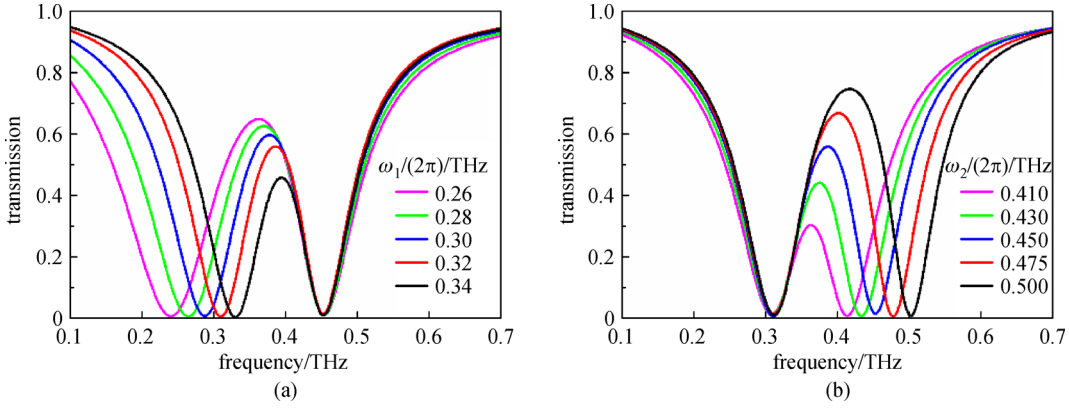

Fig. 4 Fitted transmission spectrum with different (a) ω_1 and (b) ω_2

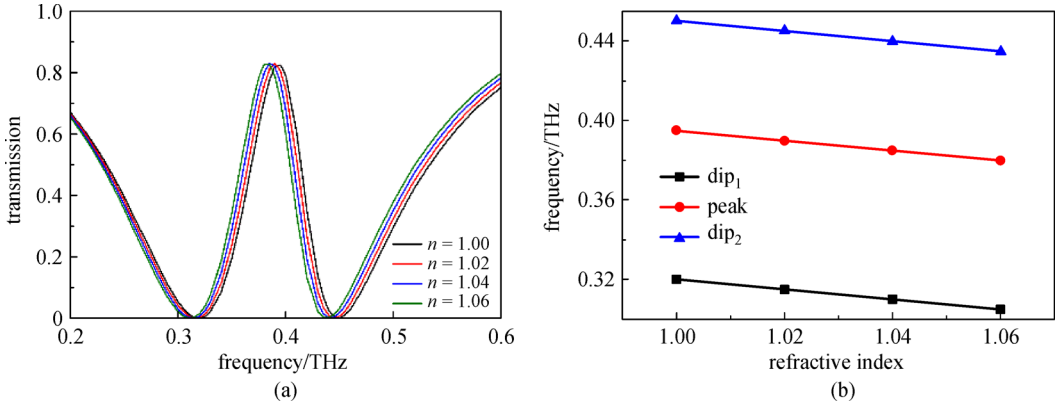

Fig. 5 (a) Spectral transmission at different refractive indices; (b) resonance frequency of dip_1/peak/dip_2 versus the refractive index

Table 1 Comparison of performance of reported EIT-based sensor

	our work	Ref. [27]	Ref. [36]	Ref. [37]	Ref. [38]
working frequency band/THz	0.1 – 0.7	1 – 3	0.4 – 0.7	20 – 36	15 – 45
sensitivity/(THz·RIU^{-1})	0.25	0.59	0.112	26.6	6.4
sensitivity ($S^* = S/f_0$)	0.633	0.32	0.164	0.85	0.285

two components along x and y axis. Both x-polarized and y-polarized light have a dip around 0.91 THz in transmission spectra. The combined impact leads to the change in line shape. The sharp and asymmetric Fano lineshape is high valuable for improving sensitivity [40]. The transmission spectra with different refraction index are shown in Fig. 6(b) when polarization angle is 60°. Refractive index increases from 1.00 to 1.15 with spacing of 0.05. The obtained sensitivity is high up to 327 GHz/RIU, which is twice as much as the above result. The sensing performance is highly improved.

Silicon bars are added to the U resonators to form closed squares, as shown by the red part in Fig. 7(a). The constant permittivity of Si is 11.7. Silicon is photosensitive whose conductivity is pump-power-dependent. A simple conductivity model of silicon is adopted. The photoconductivity δ_{Si} varies from 1 to 4000 S/m. Figure 7(b) shows evolution of transmission spectra with the conductivity of the silicon. When δ_{Si} is gradually increased, the amplitude of transparency window gradually is reduced and EIT window almost disappears at 4000 S/m. The transmittance at 0.386 THz decreases from 0.816 to 0.313. Dynamical modulation of the EIT window is realized. Define modulation depth $\Delta T/T_0 = (T_0 - T_p)/T_0$, where T_0 is the transmission of the sample without external light pump and T_p is the transmission with applied optical power. The modulation depth for peak amplitude is 61.8% when δ_{Si} = 4000 S/m. This attractive modulation may provide prospective applications in THz imaging, communications, and so on.

Strong dispersion is a remarkable characteristic of EIT response. Slow light effect is physically related to large group index which can be produced by extremely steep normal phase dispersion. Figure 7(c) depicts the simulated phase spectra at different silicon conductivity. Strong phase dispersion around the transmission window is observed. With the increase of δ_{Si}, the phase shift changes. The group delay (τ_g) can be retrieved from $\tau_g = -\mathrm{d}\varphi(\omega)/\mathrm{d}\omega$, $\omega = 2\pi f$, where $\varphi(\omega)$ is the transmission phase shift. Figures 7(d) shows the group delay as a function of frequency at different silicon conductivity. It is observed that at the resonance frequencies of ω_1 and ω_2, group delay is negative. When δ_{Si} = 1 S/m, large positive group delays are obtained around the transparency peak, indicating potential applications in slow-light devices. With increasing the conductivity, group delay is reduced. Thus flexible control on group delay and slow effect are achieved.

4 Conclusions

In conclusion, we have demonstrated EIT-like effect by two concentric USRs based on the interaction between bright-bright modes. The transparency window and dips have a redshift with the increase of USR length. Multiple resonance dips are obtained with the change of polarization angle of incident light, which can be used for multi-channel filter. Fano lineshape is observed at certain polarization angles. The polarization-sensitive property may find its applications in flexible tuning. The sensing performance based on EIT-like and Fano resonance is discussed. The sensitivity is about 327 GHz/RIU. In addition, active control on EIT-like effect is demonstrated by adding photosensitive silicon bars into unit cell. The

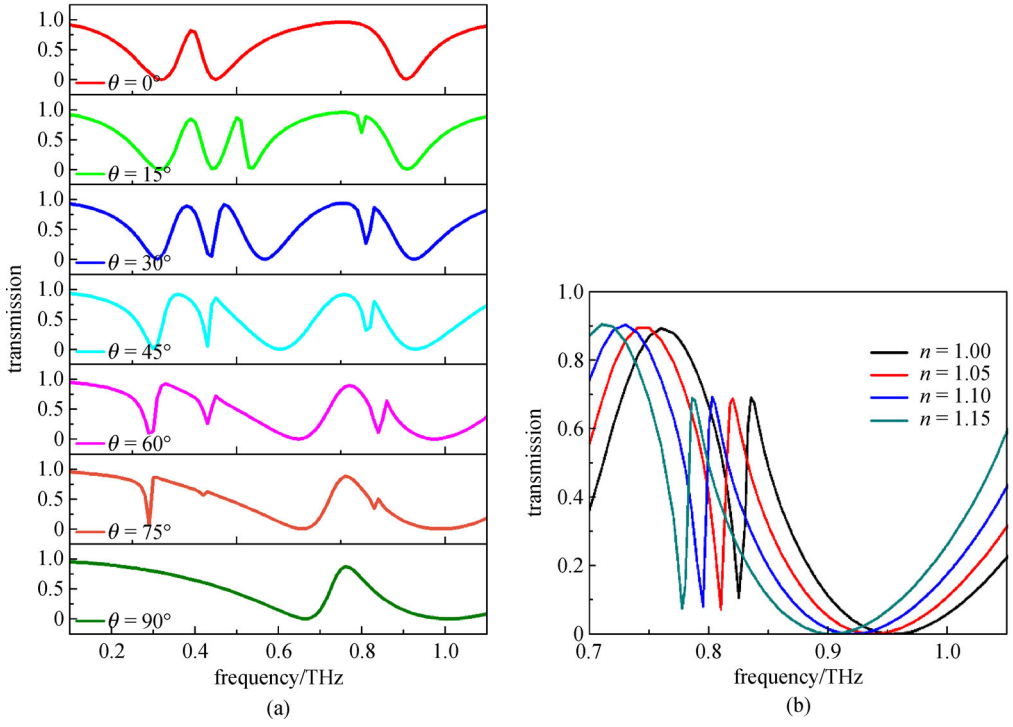

Fig. 6 (a) Transmission spectrum under different polarizations; (b) transmission spectra at different refractive indices. The polarization angle $\theta = 60°$

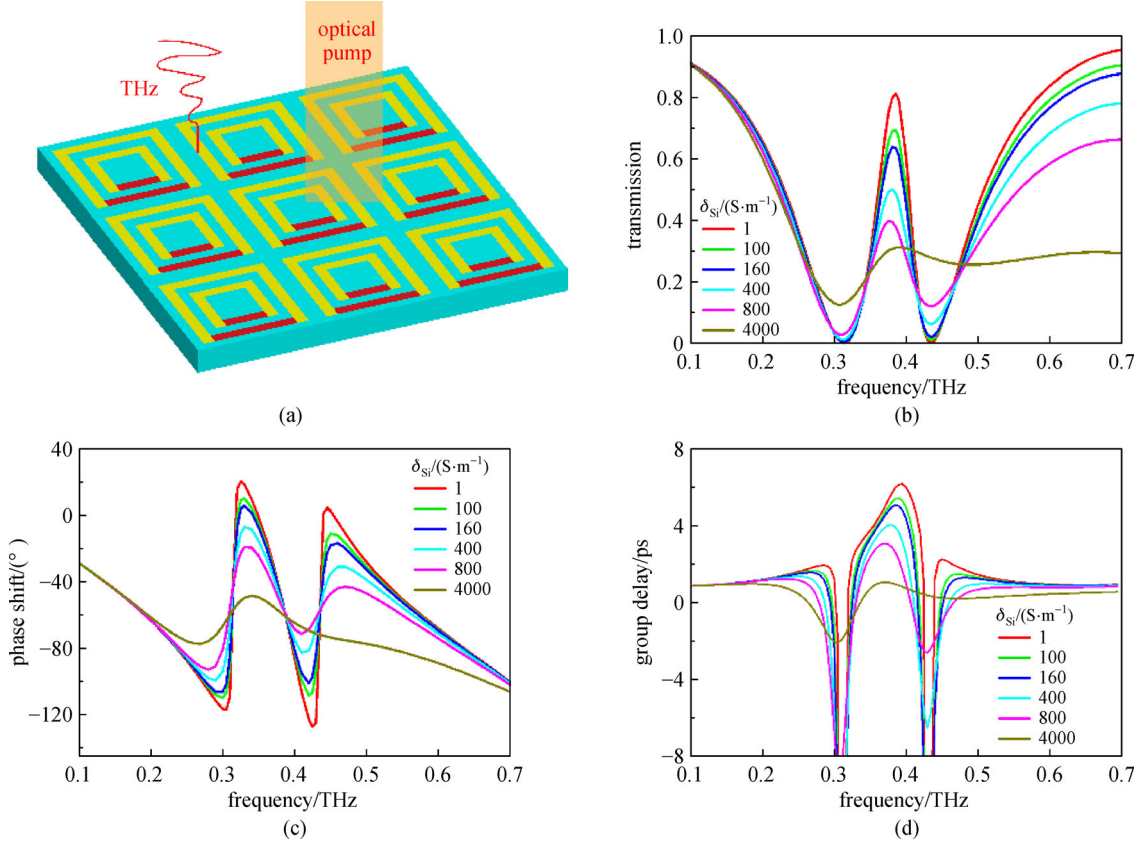

Fig. 7 (a) Geometric diagram of structure. The red region is photosensitive silicon; (b) transmission spectrum, (c) phase shift, and (d) group delay of the EIT metamaterial with increasing the conductivity δ_{Si}

amplitude and phase of EIT window are adjusted by changing the pump power. Thus dynamically modulation is achieved under photoexcitation. This property may open up a new way in designing active devices such as sensors and modulators.

Acknowledgements This work was supported by the National Natural Science Foundation of China (Grant No. 11104200) and the Natural Science Foundation of Tianjin (No. 18JCYBJC17000).

References

1. Harris S E. Electromagnetically induced transparency. Physics Today, 1997, 50(7): 36–42
2. Fleischhauer M, Imamoglu A, Marangos J P. Electromagnetically induced transparency: optics in coherent media. Reviews of Modern Physics, 2005, 77(2): 633–673
3. Vardi Y, Cohen-Hoshen E, Shalem G, Bar-Joseph I. Fano resonance in an electrically driven plasmonic device. Nano Letters, 2016, 16 (1): 748–752
4. Savo S, Casse B D F, Lu W T, Sridhar S. Observation of slow-light in a metamaterials waveguide at microwave frequencies. Applied Physics Letters, 2011, 98(17): 171907
5. Neutens P, Lagae L, Borghs G, Van Dorpe P. Plasmon filters and resonators in metal-insulator-metal waveguides. Optics Express, 2012, 20(4): 3408–3423
6. Lu H, Liu X, Wang L, Gong Y, Mao D. Ultrafast all-optical switching in nanoplasmonic waveguide with Kerr nonlinear resonator. Optics Express, 2011, 19(4): 2910–2915
7. Min C, Veronis G. Absorption switches in metal-dielectric-metal plasmonic waveguides. Optics Express, 2009, 17(13): 10757–10766
8. Wang J, Yuan B, Fan C, He J, Ding P, Xue Q, Liang E. A novel planar metamaterial design for electromagnetically induced transparency and slow light. Optics Express, 2013, 21(21): 25159–25166
9. Shelby R A, Smith D R, Schultz S. Experimental verification of a negative index of refraction. Science, 2001, 292(5514): 77–79
10. Ouedraogo R O, Rothwell E J, Diaz A R, Fuchi K, Temme A. Miniaturization of patch antennas using a metamaterial-inspired technique. IEEE Transactions on Antennas and Propagation, 2012, 60(5): 2175–2182
11. Dong Y D, Toyao H, Itoh T. Compact circularly-polarized patch antenna loaded with metamaterial structures. IEEE Transactions on Antennas and Propagation, 2011, 59(11): 4329–4333
12. Pendry J B. Negative refraction makes a perfect lens. Physical Review Letters, 2000, 85(18): 3966–3969
13. Ergin T, Stenger N, Brenner P, Pendry J B, Wegener M. Three-dimensional invisibility cloak at optical wavelengths. Science, 2010, 328(5976): 337–339
14. Zhang S, Xia C, Fang N. Broadband acoustic cloak for ultrasound waves. Physical Review Letters, 2011, 106(2): 024301
15. Meng H Y, Xue X X, Lin Q, Liu G D, Zhai X, Wang L L. Tunable and multi-channel perfect absorber based on graphene at mid-infrared region. Applied Physics Express, 2018, 11(5): 052002
16. Xia S X, Zhai X, Huang Y, Liu J Q, Wang L L, Wen S C. Multi-band perfect plasmonic absorptions using rectangular graphene gratings. Optics Letters, 2017, 42(15): 3052–3055
17. Meng H, Wang L, Liu G, Xue X, Lin Q, Zhai X. Tunable graphene-based plasmonic multispectral and narrowband perfect metamaterial absorbers at the mid-infrared region. Applied Optics, 2017, 56(21): 6022–6027
18. Xia S X, Zhai X, Wang L L, Sun B, Liu J Q, Wen S C. Dynamically tunable plasmonically induced transparency in sinusoidally curved and planar graphene layers. Optics Express, 2016, 24(16): 17886–17899
19. Xia S X, Zhai X, Wang L L, Wen S C. Plasmonically induced transparency in double-layered graphene nanoribbons. Photonics Research, 2018, 6(7): 692–702
20. Zhang S, Genov D A, Wang Y, Liu M, Zhang X. Plasmon-induced transparency in metamaterials. Physical Review Letters, 2008, 101 (4): 047401
21. Liu N, Langguth L, Weiss T, Kästel J, Fleischhauer M, Pfau T, Giessen H. Plasmonic analogue of electromagnetically induced transparency at the Drude damping limit. Nature Materials, 2009, 8 (9): 758–762
22. Zhu Y, Hu X, Yang H, Gong Q. On-chip plasmon-induced transparency based on plasmonic coupled nanocavities. Scientific Reports, 2014, 4(1): 3752
23. Lee S, Park Q H. Dynamic coupling of plasmonic resonators. Scientific Reports, 2016, 6(1): 21989
24. Yang Y M, Kravchenko I I, Briggs D P, Valentine J. All-dielectric metasurface analogue of electromagnetically induced transparency. Nature Communications, 2014, 5: 5753
25. Xiao S Y, Wang T, Liu T T, Yan X C, Li Z, Xu C. Active modulation of electromagnetically induced transparency analogue in terahertz hybrid metal-graphene metamaterials. Carbon, 2018, 126: 271–278
26. Zhang H Y, Cao Y Y, Liu Y Z, Li Y, Zhang Y P. A novel graphene metamaterial design for tunable terahertz plasmon induced transparency by two bright mode coupling. Optics Communications, 2017, 391: 9–15
27. Hu S, Liu D, Yang H L. Electromagnetically induced transparency in an integrated metasurface based on bright–dark–bright mode coupling. Journal of Physics D, Applied Physics, 2019, 52(17): 175305
28. Ren X, Ren K, Ming C. Self-reference refractive index sensor based on independently controlled double resonances in side-coupled U-shaped resonators. Sensors (Basel), 2018, 18(5): 1376
29. Singh R, Al-Naib I A I, Koch M, Zhang W. Sharp Fano resonances in THz metamaterials. Optics Express, 2011, 19(7): 6312–6319
30. Singh R, Azad A K, Jia Q X, Taylor A J, Chen H T. Thermal tunability in terahertz metamaterials fabricated on strontium titanate single-crystal substrates. Optics Letters, 2011, 36(7): 1230–1232
31. Cortie M B, Dowd A, Harris N, Ford M J. Core-shell nanoparticles with self-regulating plasmonic functionality. Physical Review B, 2007, 75(11): 113405
32. Wang Y, Leng Y B, Wang L, Dong L H, Liu S R, Wang J, Sun Y J. Broadband tunable electromagnetically induced transparency analogue metamaterials based on graphene in terahertz band. Applied Physics Express, 2018, 11(6): 062001
33. Xu Z X, Liu S Y, Li S L, Yin X X. Analog of electromagnetically induced transparency based on magnetic plasmonic artificial molecules with symmetric and antisymmetric states. Physical

Review B, 2019, 99(4): 041104
34. Ren K, Ren X, He Y, Han Q. Magnetic-field sensor with self-reference characteristic based on a magnetic fluid and independent plasmonic dual resonances. Beilstein Journal of Nanotechnology, 2019, 10: 247–255
35. Li Q M, Zhang B, Xiong W, Shen J L. Modulation of the resonance frequency in double-split ring terahertz metamaterials. Optics Communications, 2014, 323: 162–166
36. Pan W, Yan Y J, Ma Y, Shen D J. A terahertz metamaterial based on electromagnetically induced transparency effect and its sensing performance. Optics Communications, 2019, 431: 115–119
37. Huang H L, Xia H, Guo Z B, Li H J, Xie D. Polarization-insensitive and tunable plasmon induced transparency in a graphene-based terahertz metamaterial. Optics Communications, 2018, 424: 163–169
38. Liu C J, Huang Y Y, Yao Z H, Yu L L, Jin Y P, Xu X L. Giant angular dependence of electromagnetic induced transparency in THz metamaterials. EPL, 2018, 121(4): 44004
39. Manjappa M, Srivastava Y K, Cong L, Al-Naib I, Singh R. Active photoswitching of sharp Fano resonances in THz metadevices. Advanced Materials, 2017, 29(3): 1603355
40. Ren X, Ren K, Cai Y. Tunable compact nanosensor based on Fano resonance in a plasmonic waveguide system. Applied Optics, 2017, 56(31): H1–H9

Kun Ren received the M.S. degree in physics from Beijing Normal University, Beijing, China, and received the Ph.D. degree in physics from Institute of Physics, Chinese Academy of Sciences, Beijing, China. She joined Tianjin University in 2007, where she is currently an associate professor at College of Precision Instrument and Opto-electronics Engineering. From 2014 to 2015, she was a Visiting Scholar at Imperial College London, UK. Her main research interests include metamaterials, plasmonics, photonic crystals, nonlinear optics. She is the author or coauthor of more than 50 refereed journal papers.

Ying Zhang is currently working toward the M.S. degree at Tianjin University.

Xiaobin Ren received the Ph.D. degree from Beijing Normal University, Beijing, China. He is currently an associate professor at the School of Science, Tianjin University of Science and Technology, Tianjin, China. From 2014 to 2015, he was a Visiting Scholar at King's College, London, UK. His research interests include surface plasmas optics, photonic crystals, optical materials and optical technologies.

Yumeng He is currently working toward the M.S. degree at Tianjin University.

Qun Han received the M.S. degree in optics from Nankai University, Tianjin, China, in 2003, and the Ph.D. degree in physical electronics from Tianjin University, Tianjin, China, in 2006.

Since 2006, he has been with the College of Precision Instruments and Opto-electronics Engineering, Tianjin University, where he is now an associate professor. From 2011 to 2012, he was a Visiting Scholar at Missouri University of Science and Technology, Missouri, USA. His current research interests include fiber lasers and amplifiers, fiber sensors, and optical materials. He is the author or coauthor of more than 100 journal papers.

Dr. Han is a member of the Optical Society of America.